



Full Length Article

Mechanical properties and quality of plasma sprayed, functionally graded tungsten/steel coatings after process upscaling

Thilo Grammes^{*}, Ashwini Kumar Mishra, Kamil Battalov, Anisa Purwitasari, Thomas Emmerich, Jarir Aktaa

Karlsruhe Institute of Technology (KIT), Institute for Applied Materials, Hermann-von-Helmholtz-Platz 1, 76344, Eggenstein-Leopoldshafen, Germany

HIGHLIGHTS

- First measurement of elastic modulus in thin interlayers of W/EUROFER FGM.
- Linear trend of coating mechanical properties with tungsten content.
- Steel plates with channels can be coated with tungsten without severe overheating.

ARTICLE INFO

Keywords:

Instrumented indentation
Plasma-facing component
First wall
Functionally graded material (FGM)
Elastic modulus
Tungsten

ABSTRACT

The First Wall of a fusion reactor needs to withstand high heat flux as well as particle bombardment. For this, a First Wall made of steel requires a protective coating with a material that may still transfer heat for conversion to energy, such as tungsten. Its thermal expansion mismatch towards steel is overcome by vacuum plasma spraying of a functionally graded material onto the steel wall, followed by a tungsten top coat. This process was recently transferred to industry for upscaling, to develop a coating technology that can cover the large dimensions of First Wall components without deteriorating the substrate steel's properties by overheating. This work represents an instrumented indentation study of the achieved coating quality and properties, combined with microstructural analysis. Hardness profiles within coating and substrate indicate successful establishment of a linearly functionally graded material and only minor substrate overheating. The latter observation is supported by electron backscatter diffraction showing no change in the substrate's microstructure. The substrate hardness was investigated on several positions of coated plates sizing up to $500 \times 250 \text{ mm}^2$. The results indicate faster cooldown in the plate corners. Cooling channel bores that were pre-fabricated in the plates had no effect on plate hardness after coating. The elastic modulus of the coating's interlayers, determined by instrumented indentation, was found lower than predicted from bulk properties. This is attributed to the heterogeneous microstructure of the thermally sprayed coating.

1. Introduction

Future fusion reactors pose challenging operating conditions for the materials of the plasma-facing First Wall (FW). In the European Demonstration Power Plant (DEMO), this steel wall will contain cooling channels to harvest heat for energy conversion [1,2] and require a protective tungsten coating to minimise wall erosion by sputtering with high-energy particles from the fusion plasma [3–5]. In order to achieve good bonding between tungsten and steel despite their mismatch in thermal expansion coefficient, functionally graded material (FGM) can

be applied in between [6–8]. The FGM under investigation consists of several interlayers of mixed tungsten and steel that sum up to a total coating thickness of 2 mm. The mixing ratio varies over FGM thickness to create a smooth transition of properties between steel substrate and tungsten top coat. Such FGM-based coatings are able to withstand fusion-relevant high heat flux and thermal fatigue scenarios [9–11]. A fabrication process for these coatings by vacuum/low-pressure plasma spraying (VPS/LPPS) technology was developed [7,8] and successfully transferred to industry for upscaling towards fusion-relevant larger geometries.

^{*} Corresponding author.

E-mail address: thilo.grammes@kit.edu (T. Grammes).

<https://doi.org/10.1016/j.matchemphys.2023.128530>

Received 8 December 2022; Received in revised form 23 August 2023; Accepted 7 October 2023

Available online 7 October 2023

0254-0584/© 2023 The Authors. Published by Elsevier B.V. This is an open access article under the CC BY license (<http://creativecommons.org/licenses/by/4.0/>).

The development of such tungsten-based coatings is an active and challenging field and a good example of the innovation potential of fusion science. Several new coating approaches are currently being investigated that push the capabilities of existing coating technologies to new limits. Besides the vacuum-plasma sprayed coatings investigated in this study, the approach of radio-frequency inductively coupled plasma spraying recently led to a successful creation of a FGM of tungsten and 316 L steel over a thickness of 1 mm, with low porosity and no traces of oxides or brittle intermetallic phases [12]. Beyond plasma spraying, the first successful attempts to create tungsten-based coatings by cold spraying have been reported [13,14]. The cold spraying approaches still suffer from low deposition efficiencies regarding the brittle tungsten and the relatively low processing temperatures, but these challenges are increasingly addressed by using a ductile secondary phase. These developments comprise a 2 mm thick coating of mixed tungsten and tantalum with less than 1% porosity that survived high heat flux tests at 4 MW/m² [13] and mixed tungsten/EUROFER coatings on AISI 304 steel substrate, with porosity below 8% and thickness up to the millimetre range [14]. A remarkable new approach to join tungsten and steel with an FGM makes use of computational phase diagrams and diffusion simulations to find interlayer materials that will establish sufficient metallic bonding between layers and especially tungsten, and that avoids the formation of brittle intermetallic phases in the process [15]. There, joints with thickness in the millimetre were created by spark plasma sintering, comprising layers of W/VCrTi/VCrAl/FeCrAl/steel. However, they still bear potential weakness at the interfaces towards tungsten and steel, as revealed by relatively high hardness jumps across these interfaces [15]. For the other aforementioned new developments, no mechanical analysis was reported so far and none of the approaches above has yet exceeded the laboratory scale. The mechanical performance of a tungsten coating, also over larger areas, will however be crucial to its use in a fusion reactor. The present study focuses on these aspects for plasma-sprayed W/EUROFER FGMs.

A first upscaling step was recently completed, with LPPS-coated plates sizing up to 500 × 250 mm² and including cooling channels [16]. The cooling channels are essential in future First Wall panels and current manufacturing routes require them to be fabricated prior to coating [17]. They were therefore included here, to study if their presence significantly affects the heat distribution in the plates during the coating process. No coolant flow was applied during the coating process. Nevertheless, the presence of such channels during coating may, even without operating coolant flow, potentially lead to local temperature differences during the coating process. Such local temperature differences are difficult to measure directly, but if they become too high they may locally change mechanical properties, which can be tracked by investigating the substrate hardness over depth. The focus of the presented study is set on a quality analysis of these components by means of indentation. Additionally, the hardness and elastic properties of the FGM coating interlayers are assessed and the microstructure is analysed by scanning electron microscopy (SEM), including electron backscatter diffraction (EBSD).

The steel used for the coating interlayers is the reduced-activation ferritic-martensitic steel EUROFER, while the substrate steel is P92 (1.4901) because of its much higher availability. For the coating, availability was not an issue since the steel powder used here was individually pre-fabricated by gas atomisation of a small melt batch. Therefore, EUROFER was selected since it is the planned material for DEMO [18]. The pairing of a EUROFER-based coating on a P92 substrate is a relevant system for fusion-oriented studies prior to irradiation state. Both are high-chromium steels with comparable chemical composition [16,19,20], a tempered martensitic microstructure [21,22] and comparable mechanical properties under non-irradiated conditions [23–25]. Also, P92 steel is closest to EUROFER in terms of magnetic properties and is therefore a selected structural material for the ASDEX Upgrade tokamak to investigate magnetic interactions with fusion plasma [26].

In terms of coating quality, the plasma spraying process used here

could overheat the steel substrate, leading to undesired annealing, potentially recrystallisation, and alteration of mechanical properties of the steel substrate. This potential overheating introduces two dilemmas that need to be overcome in the investigation of such coatings. The first dilemma is the question of how to measure overheating. VPS coating facilities are equipped only with limited capabilities for thermocouple placement and available pyrometers are only able to survey the surface temperature. This especially limits temperature surveillance over the depth of the larger plates coated here to but a few points [16]. However, the temperature history of a part may indirectly be tracked by probing the hardness of the steel substrate after the coating process, since overheating causes annealing and change of mechanical properties of the substrate [9].

The second dilemma is that, while overheating of the bulk steel substrate is undesirable, mechanical analyses of laboratory-coated specimens indicate that minor substrate overheating correlates with improved coating adhesion [9,27]. In these studies, the strongest adhesion was found on overheated samples [27]. The overheating was verified by coarsened grain structure of the steel substrate and by reduction of its hardness to about 65% of the base value over the entire probed substrate depth [9]. In addition, an increased substrate temperature may positively correlate with reduced coating porosity and thus improved thermal diffusivity of such coatings [28]. Potentially, this dilemma may be overcome when minor substrate overheating is tolerated only close to the coated surface [9]. Therefore, in the light of the upscaling of coated parts towards fusion-relevant size, temperature management will become increasingly important in order to achieve good coating adhesion over the entire coated area.

Indentation experiments are not only a suitable means to locally test the steel substrate for overheating by tracking corresponding hardness changes [9]. For the different FGM coating interlayers, indentation testing allows to probe the achieved gradient in mechanical properties between steel and tungsten. A detailed knowledge of the FGM interlayer properties is of high interest for finite element simulations of coated First Wall components in order to predict their behaviour under fusion-relevant load conditions over elongated time scales [29]. However, the mechanical properties of individual FGM interlayers are difficult to access by conventional (e.g. tensile) testing because of the low interlayer thickness (about 240 µm [16]). Here, instrumented indentation with measurement of load over indentation depth can fill the gap and provide, alongside with hardness, first estimates of the interlayers' elastic properties [30,31]. For the EUROFER substrate, a previous instrumented indentation study on similar components found modulus values in a range of 220–250 GPa. The lower end of this range is very close to the literature value of approx. 217 GPa [6,23,25,32,33].

This work presents a detailed indentation analysis of industry-fabricated coatings with protective tungsten top layer and tungsten/EUROFER FGM interlayers on P92 steel. The coated components comprise blocks of 50 × 50 mm² coated area as well as plates with coated area of 300 × 200 mm² and 500 × 250 mm², including cooling channels. In Sections 3.1 and 3.2, profiles of Vickers hardness and elastic modulus of the 50 × 50 mm² blocks, the latter derived from instrumented microindentation, are investigated over the thickness of the coating and into the substrate material. We use microindentation here instead of the more common nanoindentation, because the latter penetrates too little material volume to find representative properties of the heterogeneous coating where individual “splat” particles of steel or tungsten measure more than 5 µm in their lowest dimension. An EBSD analysis of the coating-substrate interface is performed to interpret the observed hardness profiles. Afterwards, substrate hardness profiles on different sections of the large coated plates with cooling channels (Section 3.3), as well as SEM micrographs of the coating and coating-substrate interface (Section 3.4) are compared in order to test the homogeneity of coating quality and heat distribution in industrially coated components as well as porosity of the coating.

2. Materials and methods

During the transfer of the tungsten/EUROFER FGM coating technology to industry, several blocks of $50 \times 50 \text{ mm}^2$ area as well as plates with $300 \times 200 \text{ mm}^2$ and $500 \times 250 \text{ mm}^2$ area containing cooling channels were coated by the company COATEC GmbH (Schlüchtern, Germany) using low-pressure plasma spraying. All substrates consisted of 20 mm thick ferritic-martensitic P92 steel (1.4901) due to its higher availability and comparable properties with regard to EUROFER steel [21–26]. Details on the manufacturing can be found in Ref. [16]. The coatings with total thickness of 2 mm consist of a 1.2 mm thick FGM and a 0.8 mm thick tungsten top coat. The FGM, in turn, consists of five interlayers of mixed tungsten and EUROFER steel, with tungsten vol% (taken as vol% of the mixed powder feedstock) as detailed in Fig. 1.

For indentation analysis, cross sections of coating and substrate (Fig. 1) were prepared by electric discharge machining of specimens from the coated parts, followed by standard metallographic preparation, with last polishing step using $\varnothing 0.1 \mu\text{m}$ diamond suspension. The hardness and modulus analysis in Section 3.1 and 3.2 of this article was done on samples from the $50 \times 50 \text{ mm}^2$ blocks. The larger plates are investigated in Section 3.3 and 3.4 to test uniformity of coating properties over larger manufacturing areas.

The indentation experiments were conducted on an instrumented indenter (Zwick BZ2.5/TS15, ZwickRoell GmbH & Co. KG, Ulm, Germany) equipped with a Vickers tip, using a load of 1 kg and a holding time of 14 s, which corresponds to HV1 measurements. In addition to HV1 units (effectively kilopond/ mm^2), the hardness plots will also present a scale converted to GPa units. The minimum distance between two indentations was 500 μm . The indentation diagonal was typically between 70 and 100 μm , while “splat” particles in the coating had typical diameters of 30–50 μm and typical thickness of 5–10 μm . With the applied cross-sectional cuts, the indenter hit the splats „from the side”, thus always deforming many splats at once. Therefore, hardness and modulus data obtained here represents averaged values taking into account the heterogeneous microstructure of the coating. The deformation observed at the indentations was not visibly influenced by the anisotropic microstructure of “stacked splats”, i.e. the two diagonals of each indentation were equally long and no splats were observed to be “pushed to the side”, perpendicular of the indenter movement.

The indentation cross-sections required for Vickers hardness were obtained with an optical microscope (VHX-1000 digital microscope, Keyence, Osaka, Japan). For the hardness profiles within the steel substrate, a depth of up to 10 mm underneath the coated surface was probed. Care was taken to omit indentations from evaluation that were

misplaced or showed major disturbances in the load-depth curve. The total number of evaluated indentations on the $50 \times 50 \text{ mm}^2$ samples is 67 for the W top, 24–30 for each of the five FGM interlayers and 8–12 for the individual distances from the interface within the steel substrate (219 in total for the substrate). For the $300 \times 200 \text{ mm}^2$ plate (values in brackets for $500 \times 250 \text{ mm}^2$ plate) the total number of evaluated indentations in each of three plate positions (middle, edge, corner) is 7–12 (4–6) for the individual distances from the interface in between cooling channels and 1–5 (1–3) for the individual distances from the interface above cooling channels.

The elastic modulus, E_{IT} , was determined from a linear fit to the unloading part of the load-depth curve for each indentation, following the DIN EN ISO 14577 standard [31]. A detailed description of the analysis procedure is provided in the supporting information. The range for the linear fit was chosen as 40–98% of the test load, well within the recommendations of the DIN EN ISO 14577 standard [31]. No sample curve showed significant deviation from linearity in this range.

Electron microscopic cross sections of the coating and electron backscatter diffraction analysis of the coating-substrate interface were conducted using a scanning electron microscope (EVO MA10, Zeiss, Oberkochen, Germany, equipped with EBSD detector e-Flash HR+, Bruker Nano GmbH, Berlin, Germany). The specimens for EBSD analysis were prepared by standard metallographic means until $\varnothing 1 \mu\text{m}$ diamond suspension and subsequently vibro-polished for up to 18 h using an Al_2O_3 suspension ($\varnothing 0.05 \mu\text{m}$). For the EBSD measurement the specimens were tilted by 70° to the electron beam.

3. Results and discussion

3.1. Hardness profile of coated small blocks

Fig. 2a displays the hardness profile from coating (left) to substrate (right) for the $50 \times 50 \text{ mm}^2$ block samples. Green circles and black squares correspond to hardness before and after the coating process, respectively. Horizontal dashed lines indicate literature values for the hardness of recrystallised bulk tungsten [34] and heat-treated EUROFER after austenitisation at 980°C and subsequent annealing at 760°C [35]. These literature values serve as a rough orientation only, because hardness of a metal depends strongly on its thermal history.

The mean substrate hardness after coating was about 85–90% of the value before coating and showed a slight decrease towards the coating-substrate interface, but within error margin (Fig. 2, right side) and thus much less pronounced than the hardness jump found in a previous study (85–90% of base hardness here versus 65% of base hardness in Ref. [9]). The overall low hardness decrease of the substrate indicates that the substrate temperature mostly remained below the annealing temperature of the steel ($750\text{--}780^\circ\text{C}$ [24]). This is, in general, a desirable outcome and in line with thermocouple measurements done during calibration of the coating process ($695\text{--}752^\circ\text{C}$ [16]).

Within the FGM, the hardness increased with each interlayer from steel to W top layer (Fig. 2, left side), indicating successful achievement of a functional grading. Fig. 2b shows the hardness of the coating layers over their analysed tungsten content (energy-dispersive X-ray analysis, EDX, from Ref. [16]). The aimed-for linear gradient of hardness over the coating layers was well achieved. A linear fit to the data in Fig. 2b yielded $\text{HV} = 1.60 \cdot (\text{at}\% \text{W}) + 189.08$ with $R^2 = 0.995$. The hardness of the tungsten top layer is comparable to the one found in a previous, laboratory-produced development step of such coatings [7] and, coincidentally, very close to the hardness of recrystallised bulk tungsten [34]. It needs to be stressed, however, that the tungsten top layer here cannot be seen as equal to recrystallised bulk tungsten as the route of manufacturing and microstructures are different.

We note that the hardness of the first two interlayers adjacent to the steel substrate lies slightly below the substrate hardness as well as in the hardness range of pure EUROFER [35], even though the layers contain significant amounts of tungsten. Porosity in the coating layers could

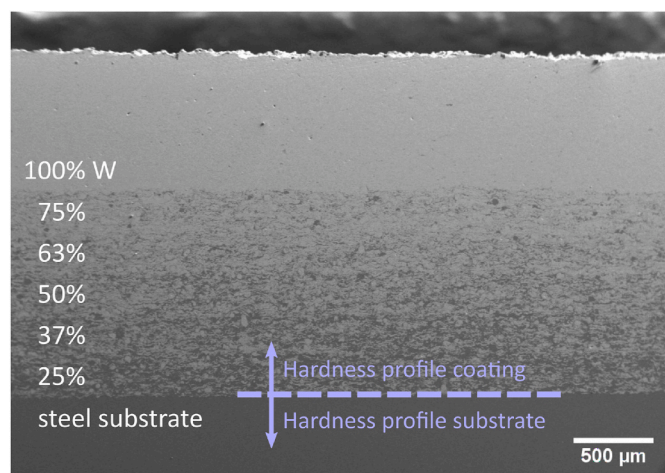


Fig. 1. Cross section of the coating with indication of the coating-substrate interface. The interlayers with different tungsten content (vol%) are highlighted.

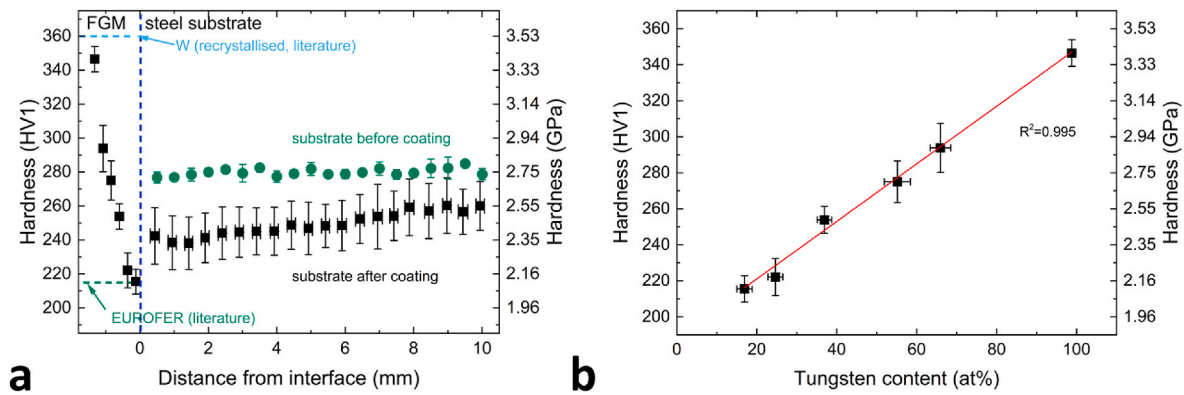


Fig. 2. (a) Vickers hardness profile from coating to steel substrate ($50 \times 50 \text{ mm}^2$ block sample). The vertical dashed line marks the coating-substrate interface, with data to the left corresponding to the W top and the five FGM interlayers and data to the right corresponding to hardness profiles within the steel substrate. Green circles show substrate hardness prior to coating, black squares after coating process. Error bars show 95% confidence intervals. Horizontal dashed lines show literature hardness values for recrystallised tungsten [34] and for annealed EUROFER [35] and serve as a rough guidance only. (b) Vickers hardness of the five coating interlayers and the tungsten top coating versus analysed tungsten content. The straight line represents a linear fit with R^2 value indicated. (For interpretation of the references to colour in this figure legend, the reader is referred to the Web version of this article.)

theoretically cause a hardness reduction, but the porosity found in the present coatings is deemed too low to have such effect [16]. A more likely reason for the observed step in hardness would be that the substrate may have actually undergone additional softening in the first few tens of micrometers underneath the interface, since here with the arrival of melt droplets during plasma spraying a significantly increased local heat input could be possible. This was not tracked with the present hardness measurements because the first substrate indentation was set $500 \mu\text{m}$ away from the interface to avoid accidental deformation of the first tungsten/steel interlayer, which would in turn have tampered with the indentation result.

However, any direct comparison to the substrate hardness is difficult since the involved steels differ (EUROFER for the coating, P92 for the substrate) and the hardness depends on thermal and mechanical history of the materials. Especially the thermal history differs a lot here. The substrate was annealed and subsequently suffered heat input during the coating process. The steel within the coating rapidly was cooled from melt droplet state. Under such conditions, hardness differences may well be expected.

Fig. 3 shows an EBSD pattern, measured from the coating (left) towards the steel substrate (right) of a $50 \times 50 \text{ mm}^2$ block sample. The coating is dominated by small, equiaxed grains whereas the steel substrate displays a lath structure typical for the ferritic-martensitic steels P92 and EUROFER [21,22,36,37]. This ferritic-martensitic microstructure was preserved even very close to the coating interface, thus

supporting the above finding of little to no hardness change in the substrate. The small grain size in the coating may stem from rapid solidification of molten droplets during the coating process [38].

3.2. Elastic modulus profile of coated small blocks

Fig. 4a shows the profile of elastic modulus from indentation, E_{IT} , through the thickness of the coating and into the steel substrate of the $50 \times 50 \text{ mm}^2$ block samples. The modulus in the steel substrate remained constant over the substrate depth (Fig. 4, right). Summarising over all 216 indentations in steel, the mean E_{IT} of the substrate after the coating process was $226 \pm 18 \text{ GPa}$ (standard deviation) which is in good agreement with the room temperature literature value of 217 GPa for P92 steel (green horizontal dashed line Fig. 4a) [24]. Prior to coating the modulus of the P92 substrate was slightly higher (237 GPa , green circle in Fig. 4) than the literature value, but within error margin of the value after coating. Judging from this, the determination of modulus data from indentation experiments appears to be reliable here and will be extended onto the coating.

Additionally, the literature elastic modulus of EUROFER was indicated in Fig. 4a (horizontal green dashed line, approx. 217 GPa) [32,33,39]. At this point we note that the literature modulus of EUROFER is practically identical to the room temperature modulus of similar steels such as P92 and F82H [24,25,33,40–43]. A close scrutiny of the literature reveals that the value of 217 GPa always traces back to values

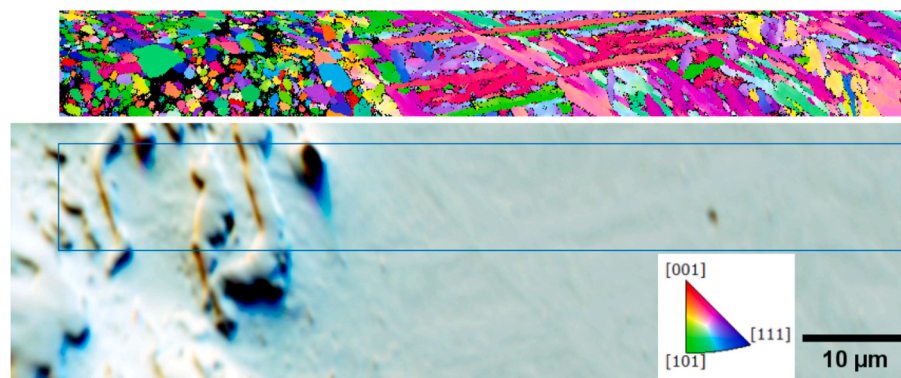


Fig. 3. EBSD pattern (top) and corresponding SEM view (bottom) ranging from the coating (left) to the steel substrate (right) on a $50 \times 50 \text{ mm}^2$ block sample. EBSD colours correspond to the crystal orientation by X-inverse pole figure. Black regions in EBSD pattern are non-indexed areas. The coating is dominated by small, equiaxed grains while the steel substrate displays a lath structure. (For interpretation of the references to colour in this figure legend, the reader is referred to the Web version of this article.)

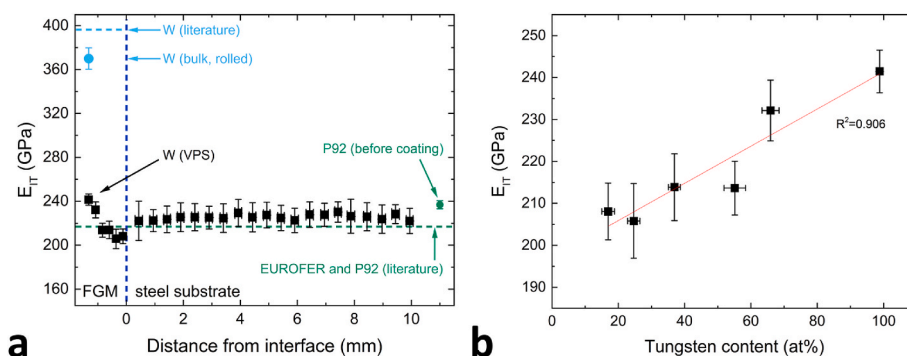


Fig. 4. (a) Profile from coating to steel substrate showing the elastic modulus E_{TT} probed by instrumented indentation ($50 \times 50 \text{ mm}^2$ block sample). The vertical dashed line marks the coating-substrate interface, with data to the left corresponding to the W top and the five FGM interlayers and data to the right corresponding to measurements within the steel substrate. Horizontal dashed lines mark literature values of elastic modulus for bulk tungsten, and P92 and EUROFER steels [24,32,33,39,44,45]. The blue and green circles show data measured on rolled bulk tungsten and on a P92 block prior to coating, respectively. Error bars show 95% confidence intervals. (b) Elastic modulus of the five coating interlayers and the tungsten top coating versus analysed tungsten content. The straight line represents a linear fit with R^2 value indicated. (For interpretation of the references to colour in this figure legend, the reader is referred to the Web version of this article.)

reported by Tavassoli et al. upon collecting data for an ITER materials database, and these values were explicitly reported in Ref. [25] to be taken from F82H steel as a placeholder since no reliable data was yet available for EUROFER [25,40–42]. A more recent publication includes 2018 data of the RCC-MRx code for EUROFER [33], again showing the same value of 217 GPa for both EUROFER and F82H. One may therefore expect that the real modulus of EUROFER will indeed be close to that of other ferritic-martensitic steels such as F82H or P92. However, considering the importance of EUROFER for nuclear fusion, the rather limited development of the database over the years for such a fundamental property as elasticity is striking and probably may be attributed to the low availability of EUROFER. Therefore, we conclude that there is a high need for every new attempt to gain insight into the elasticity of fusion materials, such as the coating modulus we study here.

The modulus of the coating increased from the coating-substrate interface towards the tungsten top layer, roughly following a linear trend. Fig. 4b shows this trend of modulus over the analysed tungsten content of the coating's interlayers (EDX data from Ref. [16]). A linear fit to this data (Fig. 4b) yielded $E_{TT} = 0.44 \cdot (\text{at\% W}) + 197.06$. This fit only has a coefficient of determination of $R^2 = 0.906$, with the values for 50–80 at% tungsten differing the most. However, no more refined fitting model was considered to yield a significant increase in information gain taking into account the error margin of the modulus measurement. The linear fitting model is in line with the rule of mixture, since the ratio of tungsten/steel vol% of the interlayers was changed linearly. However, the absolute modulus values measured in the coating were much lower than expected from literature. The literature modulus value for bulk tungsten is 396 GPa [44,45], about 1.6 times higher than the E_{TT} value of 241 GPa measured here for the VPS tungsten top coating. In order to verify that this low modulus is not an artefact of the indentation method, several bulk pieces of rolled tungsten were investigated by the same method, resulting in an average modulus of 370 GPa (blue circle in Fig. 4). This is close to the literature value, albeit slightly lower.

The slight reduction could be caused by minor cracks generated by indentation of the bulk tungsten with HV1 load (9.81 N). At this point we need to point out that the value of 396 GPa which is the current standard within the EUROFUSION project [44], was not determined by indentation. It represents a best-of value from different reports using both tensile testing and ultrasonic analysis. Despite this limitation where the literature values vary widely, we note that, among these literature values, the value reported from tensile testing (357 GPa) [46] is almost within error margin of the value we found for bulk rolled tungsten (see above). Therefore, the measurements presented here are able to reproduce literature values. Furthermore, they provide additional modulus data for fusion materials and thus help to establish a more profound database for this field where reliable material properties are still sparse.

The much lower values found for the VPS tungsten most likely result from the VPS microstructure, consisting of stacks of disk-shaped particles and pores [16], rather than a dense bulk material. Even though such a VPS microstructure may still provide significant resistance towards indentation and thus display hardness similar to bulk values (Fig. 2), its elastic response may be expected to be more compliant. Similar modulus reductions compared to bulk material have been found for indentation tests on a variety of metallic, ceramic and cermet coatings produced by thermal spraying [47–50]. This has been attributed to weak spots such as pores, cracks, unmelted particles, oxides and weak boundaries between individual disk-shaped particles [47–50]. Nohava et al. have noted an effect of the indentation depth on Young's modulus, with decreasing modulus for increasing depth until a saturation is reached at high depths. They have attributed this to the activation of an increasing number of the aforementioned weak spots [50]. The indentation depths probed in this work ($>9 \mu\text{m}$) are within the saturation range found by Nohava et al. for stainless steel [50]. Thus, the indentations here are regarded as big enough to deliver characteristic properties of the coating. Modulus reductions for plasma sprayed tungsten were not only found by indentation but also by means of four-point bending: Kovarik et al. tested radio frequency inductively-coupled plasma sprayed pure tungsten layers with significant porosity ($>10\%$) by four-point bending. They reported elastic modulus values of 200 GPa and below, compared to 430–450 GPa for a reference rolled tungsten sheet [51].

The coatings studied here include unmelted particles and porosity [16]. Additionally, the presence of some poor intersplat contacts as well as minor amounts of oxide film between some disk-shaped particles, despite the vacuum process, cannot be completely excluded. The observed drop in modulus compared to bulk material, although still surprisingly high, is attributed to all of these defects in line with the abovementioned literature. This should not be seen as a weakness of the coating. Indeed, a higher compliance as result of porosity and low modulus could increase the damage tolerance of such coatings in a reactor environment with cyclic thermal loads, since larger strains may be tolerated before critical stresses are reached.

3.3. Hardness analysis of larger coated plates

To test the homogeneity of process heat distribution, two industry-coated plates sizing $300 \times 200 \text{ mm}^2$ and $500 \times 250 \text{ mm}^2$ including cooling channels [16] were investigated for substrate hardness at several positions. A previous ultrasonic immersion analysis of these plates has indicated adhesion of the coating, with ultrasonic echoes from underlying cooling channels not being blocked by any interfacial defects [16]. Nevertheless, the ultrasonic analysis of the $300 \times 200 \text{ mm}^2$ plate has indicated potential interface defects or weaker bonding at the corners

and edges of the plate. The larger plate sizing $500 \times 250 \text{ mm}^2$ was coated later, so that parameters could already be optimised. Therefore, no similar ultrasonic "weak spot" features were found for the $500 \times 250 \text{ mm}^2$ plate [16]. The difference of ultrasonic signals in corners compared to the middle of the plate could potentially be caused by lower substrate temperature in the corners, since the quality of layer adhesion depends on the substrate temperature during coating [9,27]. To investigate this, specimens were cut from three different regions of each plate (A,B,C, Fig. 5a). Regions A and B both contain cooling channels and are located at a short edge (A) and in the middle of the plates (B), respectively. By comparing them, potential differences in coating quality along the cooling channels can be identified. Region C is located at a corner of the plates.

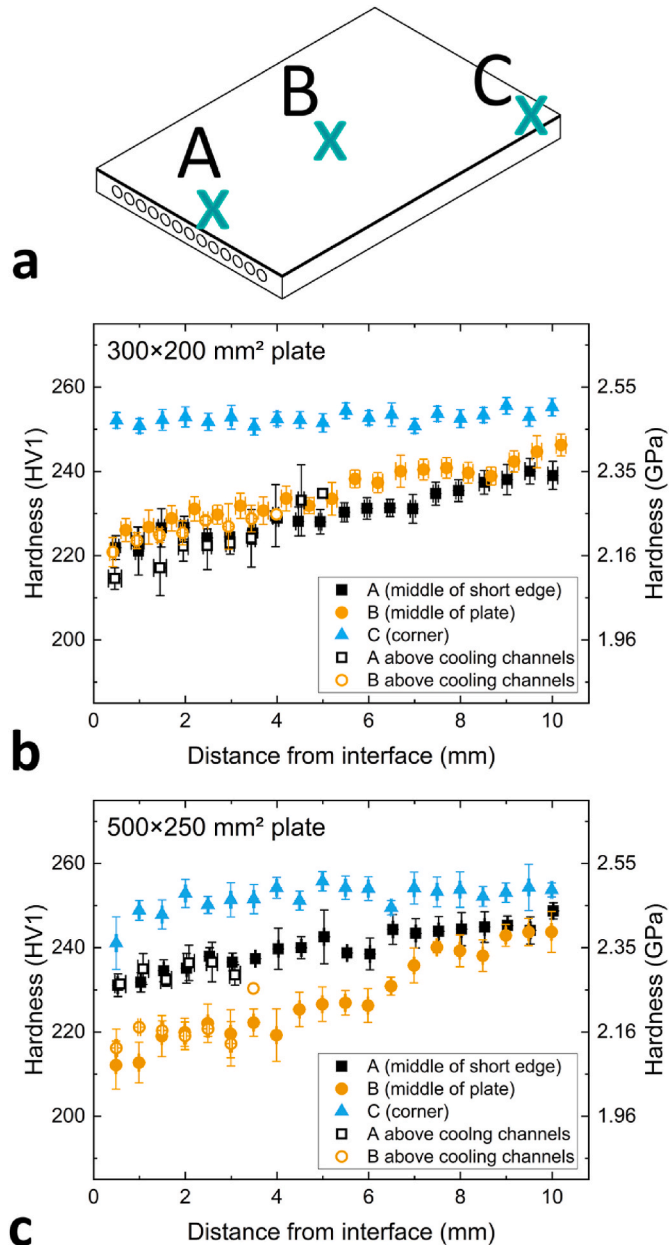


Fig. 5. (a) Schematic of a coated $300 \times 200 \text{ mm}^2$ plate with markers showing positions where samples were extracted for hardness tests. (b,c) Substrate hardness profiles below coating-substrate interface for (b) $300 \times 200 \text{ mm}^2$ plate and (c) $500 \times 250 \text{ mm}^2$ plate. Measurements are taken from positions A, B and C as shown in (a). Open symbols show measurements above cooling channels, closed symbols show measurements in channel walls. Error bars show 95% confidence intervals.

Several hardness profiles of the steel substrate were measured on each specimen following the same procedure as above. For regions A and B, some hardness profiles were positioned above cooling channels and thus stop at a depth of 4 mm below the coating-substrate interface, where the channels begin. The comparison of profiles above channels and within channel walls allowed to search for potential zones of local overheating. The results, however, show similar hardness profiles above cooling channels and in channel walls (open and closed symbols in Fig. 5, respectively). As a conclusion, the presence of pre-fabricated cooling channels in the plates did not negatively affect the temperature distribution during the coating process. This is a positive outcome since it takes one technological challenge out of a still very complex development project. In future development steps towards full-scale reactor components, one may counter additional heating up by using active substrate cooling within the coating facility. Even the already present cooling channels could be utilized for this. However, for the present development state, such active cooling was still out of scope since it requires substantial investment in specialised coating facilities. This will be needed eventually for the realisation of fusion energy.

For the $300 \times 200 \text{ mm}^2$ plate, the hardness profiles measured in regions A and B were similar (black squares and orange circles in Fig. 5b), indicating constant quality of coating over the length of the plate. For the $500 \times 250 \text{ mm}^2$ plate, region A displayed higher hardness than region B, indicating faster cooling at the plate's edge (Fig. 5c). Following this idea, the plate middle B underwent more profound softening because heat removal was slower here. The corner region C in both plates showed constant high hardness of approx. 252 HV1 over the entire probed depth (Fig. 5). The lowest hardness values in regions A and B were at approximately 85–90% of this value and were found close to the coating-substrate interface for regions A and B of the smaller plate and for region B of the larger plate. This is qualitatively similar to the hardness profile observed on the $50 \times 50 \text{ mm}^2$ blocks (Fig. 2). The base hardness reported for the $50 \times 50 \text{ mm}^2$ blocks is slightly higher (277 HV1, Fig. 2a) but the hardness reduction was to 85–90% of this level, too. The EBSD analysis below in Section 3.3 also confirms similar substrate microstructure for blocks and plates. The higher base hardness of the smaller blocks is assumed to be caused by variations in thermal history during the - nominally identical - initial heat treatment prior to coating that may be caused by the very differently sized pieces or by position within the annealing furnace.

The decreasing hardness towards coating-substrate interface indicates a slight overheating of the steel close to the interface. Such a local overheating is a preferred outcome since a moderately increased temperature close to the interface is considered beneficial for coating adhesion [9,27].

At 10 mm depth below the interface, the hardness in regions A and B has increased towards the constant value of region C, albeit still being slightly lower for the smaller plate and for region B of the larger plate (Fig. 5). This indicates that these regions were subjected to minor softening up to high depth. However, the corresponding heat input was low enough that the ferritic-martensitic microstructure of the substrate was preserved, as will be shown in Section 3.4. Future coating iterations will attempt to further push this softening to within just a few millimetres below the interface, in order to maintain bulk properties of the coated component.

During processing the plates were only heated by spray guns. The meandering movement of the guns allows for inhomogeneous cooldown of the plates, with corners and edges being able to cool down faster. The corner temperature of $500 \times 250 \text{ mm}^2$ plates was measured to be about $30\text{--}50 \text{ }^\circ\text{C}$ below the temperature in the middle of the plates [16]. This is confirmed by the hardness profiles in corners and edges. Only for the $300 \times 200 \text{ mm}^2$ plate the edges apparently still had a temperature similar to the middle since here no hardness difference was found. The high hardness at the corners supports the ultrasonic indications of weak spots found there for the $300 \times 200 \text{ mm}^2$ plate [16]. However, for the $500 \times 250 \text{ mm}^2$ plate a more homogeneous ultrasonic response was

found [16], despite the difference in hardness profiles. This indicates that other process parameters may play a role as well, or that ultrasonic testing is less sensitive to local overheating than hardness analysis.

Although the overall hardness decrease was low (to 85–90% of the base value), the qualitative trends found here highlight the importance of temperature management when upscaling thermal spray coating processes. Potentially, a more homogeneous distribution of substrate properties over the coated area may be achieved by additional heating of the corners and edge zones during the coating process.

3.4. Microstructural analysis of larger coated plates

To further track differences between corners and middles of the coated plates, the microstructure of coating and coating-substrate interface in these regions was analysed by SEM and EBSD. Figs. 6 and 7 show representative SEM micrographs for the 300×200 and 500×250 mm² plates, respectively, with letters “B” and “C” indicating middle and corner of the plates as drafted in Fig. 5.

The targeted coating layer structure was successfully achieved, with five W-EUROFER interlayers and a thick tungsten top coating (Fig. 6 B1, C1 and Fig. 7 B1,C1). When compared to the 50×50 mm² samples [16], the coated 300×200 and 500×250 mm² plates display a higher degree of porosity, as well as multiple unmelted tungsten particles (brighter gray particles of round shape). The porosity is exemplified in Fig. 6 B2, C2 and Fig. 7 B2,C2 for the W top coating of the plates. The porosity of this W top coating was evaluated from SEM image analysis using the method described in Ref. [16]. A porosity of $2.3 \pm 0.9\%$ was found (area % of the evaluated images). In total, 20 images of $1060 \times$ magnification were evaluated: five from each of the middle and corner regions of the 300×200 and 500×250 mm² plates. No significant differences in porosity level were observed between the individual regions (individual porosities of the regions: $2.3 \pm 0.9\%$, $2.9 \pm 0.3\%$, $1.4 \pm 0.3\%$, $2.4 \pm 1.1\%$ for 300×200 B,C and 500×250 B,C, respectively). These numbers are within a typical porosity range for plasma-sprayed coatings, including previous lab-scale iterations of the studied tungsten-steel layers as well as comparable developments by atmospheric plasma

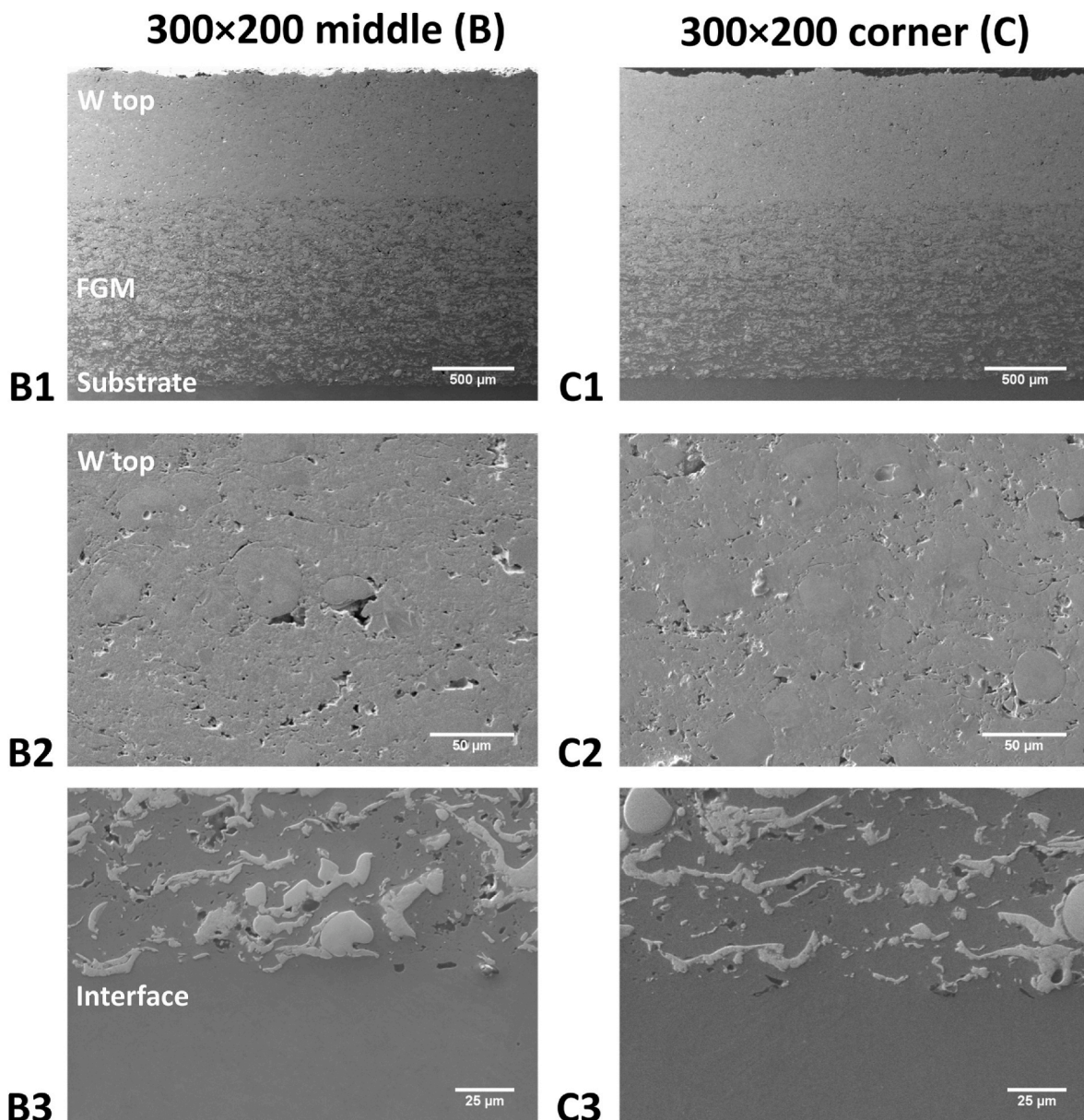


Fig. 6. SEM micrographs of the coating on a 300×200 plate. (B1-3) Plate centre “B”. (C1-3) Plate corner “C”. (B1, C1) Overview of entire coating, with visible FGM grading and W top layer. (B2, C2) W top layer with porosity visible. (B3, C3) Close-up view of coating-substrate interface with porosity.

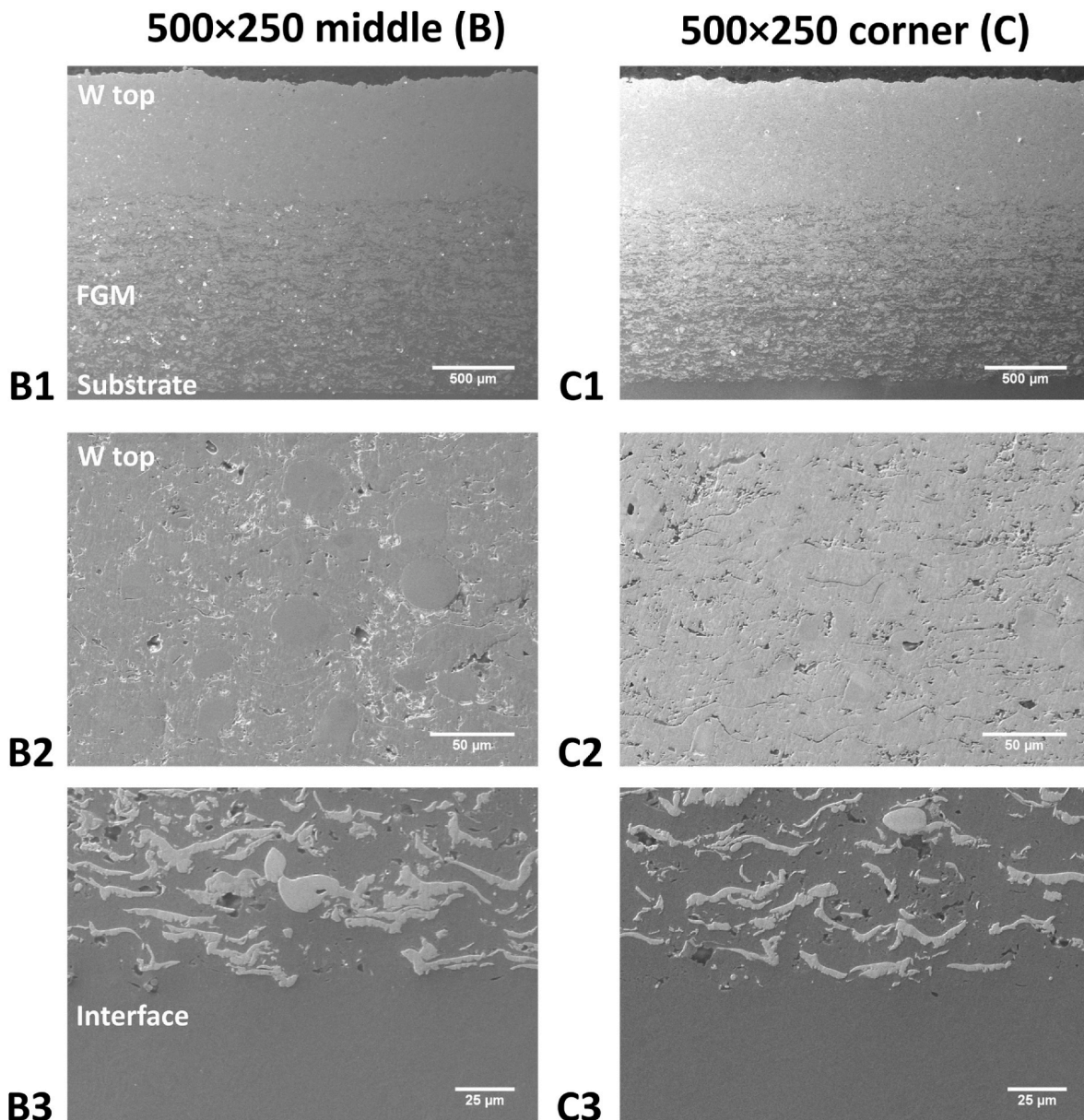


Fig. 7. SEM micrographs of the coating on a 500×250 plate. (B1-3) Plate centre "B". (C1-3) Plate corner "C". (B1, C1) Overview of entire coating, with visible FGM grading and W top layer. (B2, C2) W top layer with porosity visible. (B3, C3) Close-up view of coating-substrate interface with porosity.

spraying [39,52,53]. We note that the porosity of 2.3% is more realistic than the one we previously found for the coating on the 50×50 mm² blocks [16]. This previously published, lower porosity value is probably caused by differences in the sample polishing procedure.

At the coating-substrate interface, however, only minor porosity was observed for the plates (Fig. 6 B3,C3 and Fig. 7 B3,C3), with interface quality being comparable to that found earlier for the 50×50 mm² blocks [16]. The porosity at the interface is not easily quantifiable because of the interface's irregularity, but as a general observation, the porosity adjacent to the steel substrate was lower than the one observed just above in the FGM. Exemplarily, the interface was tracked by taking several SEM micrographs along the length of the SEM samples for middle and corner region of the 300×200 mm² and 500×250 mm² plates to visualise the interface quality. The corresponding image series are representative for the respective samples, with at least 3.6 mm length of interface captured for each series. The image series are provided in the supporting information. Here, no significant differences were observed between middle and corners of the plates. Notably, there

were no signs of interface cracking or other particularly weak spots in the corner regions of the plates.

An EBSD analysis just underneath the coating-substrate interface was conducted for the middle and corner regions of the 300×200 and 500×250 mm² plates. The resulting patterns are similar for all four regions (Fig. 8) and qualitatively match the one found for the smaller 50×50 mm² blocks (Fig. 3). They all show small, equiaxed grains in the coating, while in the substrate the ferritic-martensitic lath structure with elongated grains was preserved. This supports the above interpretation from hardness analysis that the overheating during plasma spraying was low enough that the ferritic-martensitic microstructure of the substrate was preserved.

Recalling the ultrasonic analysis of these plates [16], a potential weak spot found back then in the corner of the 300×200 mm² plate cannot be confirmed by this microstructural analysis, since neither interface porosity nor substrate microstructure indicate differences between middle and corner. This highlights that single features in ultrasonic analysis of such coatings cannot simply be translated to presence

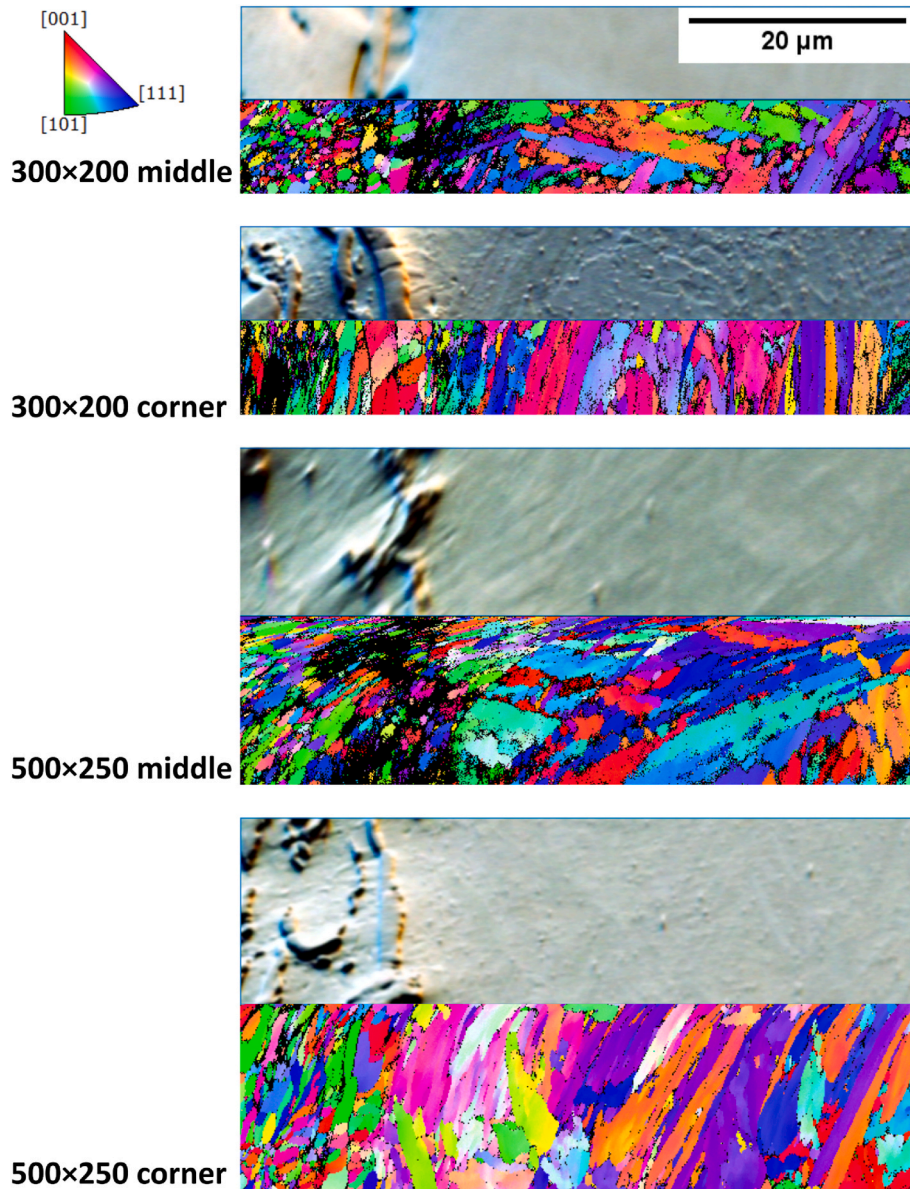


Fig. 8. EBSD analysis for middle and corner regions of coated $300 \times 200 \text{ mm}^2$ and $500 \times 250 \text{ mm}^2$ plates, ranging from the coating (left) to the steel substrate (right). Top figures of each image pair show SEM view, bottom pictures show EBSD patterns with colours corresponding to the crystal orientation by X-inverse pole figure. Black regions in EBSD patterns are non-indexed areas. In all four cases, the coating is dominated by small, equiaxed grains while the steel substrate displays a lath structure. (For interpretation of the references to colour in this figure legend, the reader is referred to the Web version of this article.)

of microstructural weak spots.

The results of this microstructural analysis indicate that the coating quality was relatively homogeneous over the area of the plates, besides the aforementioned need for improved temperature management in the corner regions. They also indicate that a minor overheating of the substrate, as was necessary to cause the minor hardness reduction observed in Fig. 5, is still feasible without impairing the ferritic-martensitic substrate microstructure that is desired for operation in a fusion reactor.

4. Conclusions

This work presents a combined indentation and microstructure analysis of functionally graded tungsten/steel coatings that were plasma sprayed onto steel substrates sizing up to $500 \times 250 \text{ mm}^2$ in area. Hardness profiles in the coating demonstrate achievement of functional grading while hardness profiles in the substrate show that substrate overheating, if present, was low and most pronounced close to the

coating-substrate interface. An overall low hardness loss of the substrate is supported by EBSD measurements indicating no change of substrate microstructure. Profiles of elastic modulus were determined from instrumented indentation unloading data. The modulus of the steel substrate agrees well with literature while the coating modulus is strongly reduced, presumably by defects in the coating. Hardness profiles from different positions within larger coated plates with cooling channels show that the channel bores had no negative effect in terms of substrate overheating. The corners of the plates displayed higher substrate hardness and remain potential weak spots. Taken together, this study indicates that functionally graded tungsten/steel coatings can be fabricated on large areas without excessive heat accumulation, while requirements for further improvement of heat management are identified.

CRediT authorship contribution statement

Thilo Grammes: Conceptualization, Investigation, Formal analysis, Software, Validation, Visualization, Writing - original draft, Writing - review & editing. **Ashwini Kumar Mishra:** Investigation, Formal analysis, Visualization, Writing - review & editing. **Kamil Battalov:** Investigation, Formal analysis. **Anisa Purwitasari:** Investigation, Formal analysis. **Thomas Emmerich:** Resources, Conceptualization, Writing - review & editing. **Jarir Aktaa:** Supervision, Funding acquisition, Conceptualization, Writing - review & editing.

Declaration of competing interest

The authors declare that they have no known competing financial interests or personal relationships that could have appeared to influence the work reported in this paper.

Data availability

Data will be made available on request.

Acknowledgements

TG would like to thank Alexander Valentin Brabänder (formerly KIT IAM) for discussions on indentation testing, Mathias Jetter and Ermile Gaganidze (both KIT IAM) for exchange on material properties and Roman Buchheit (formerly Leibniz INM) for input on data analysis with Python. AM thanks Dimitri Litvinov (KIT IAM) for discussions on electron microscopy.

This work has been carried out within the framework of the EUROfusion Consortium, funded by the European Union via the Euratom Research and Training Programme (Grant Agreement No 101052200 — EUROfusion). Views and opinions expressed are however those of the author(s) only and do not necessarily reflect those of the European Union or the European Commission. Neither the European Union nor the European Commission can be held responsible for them.

Appendix A. Supplementary data

Supplementary data to this article can be found online at <https://doi.org/10.1016/j.matchemphys.2023.128530>.

References

- [1] L. Barucca, E. Bubelis, S. Ciattaglia, A. D'Alessandro, A.D. Nevo, F. Giannetti, W. Hering, P. Lorusso, E. Martelli, I. Moscato, A. Quartararo, A. Tarallo, E. Vallone, Pre-conceptual design of EU DEMO balance of plant systems: objectives and challenges, *Fusion Eng. Des.* 169 (2021), 112504, <https://doi.org/10.1016/j.fusengdes.2021.112504>.
- [2] F. Arbeiter, Y. Chen, B.-E. Ghidersa, C. Klein, H. Neuberger, S. Ruck, G. Schlindwein, F. Schwab, A. von der Weth, Options for a high heat flux enabled helium cooled first wall for DEMO, *Fusion Eng. Des.* 119 (2017) 22–28, <https://doi.org/10.1016/j.fusengdes.2017.04.083>.
- [3] D. Smith, Physical sputtering model for fusion reactor first-wall materials, *J. Nucl. Mater.* 75 (1978) 20–31.
- [4] K. Ehrlich, The development of structural materials for fusion reactors, *Philos Trans R. Soc A* 357 (1999) 595–617, <https://doi.org/10.1098/rsta.1999.0343>.
- [5] M. Rieth, S.L. Dudarev, S.M.G. de Vicente, J. Aktaa, T. Ahlgren, S. Antusch, D.E. J. Armstrong, M. Balden, N. Baluc, M.-F. Barthe, W.W. Basuki, M. Battabyal, C. S. Beccuart, D. Blagoeva, H. Boldyryeva, J. Brinkmann, M. Celino, L. Ciupinski, J. B. Correia, A.D. Backer, C. Domain, E. Gaganidze, C. García-Rosales, J. Gibson, M. R. Gilbert, S. Giusepponi, B. Gludovatz, H. Greuner, K. Heinola, T. Höschen, A. Hoffmann, N. Holstein, F. Koch, W. Krauss, H. Li, S. Lindig, J. Linke, Ch Linsmeier, P. López-Ruiz, H. Maier, J. Matejíček, T.P. Mishra, M. Muhammed, A. Muñoz, M. Muzyk, K. Nordlund, D. Nguyen-Manh, J. Opschoor, N. Ordás, T. Palacios, G. Pintsuk, R. Pippan, J. Reiser, J. Riesch, S.G. Roberts, L. Romaner, M. Rosiński, M. Sanchez, W. Schulmeyer, H. Traxler, A. Ureña, J.G. van der Laan, L. Veleva, S. Wahlberg, M. Walter, T. Weber, T. Weitkamp, S. Wurster, M.A. Yar, J. H. You, A. Zivelonghi, Recent progress in research on tungsten materials for nuclear fusion applications in Europe, *J. Nucl. Mater.* 432 (2013) 482–500, <https://doi.org/10.1016/j.jnucmat.2012.08.018>.
- [6] T. Weber, J. Aktaa, Numerical assessment of functionally graded tungsten/steel joints for divertor applications, *Fusion Eng. Des.* 86 (2011) 220–226, <https://doi.org/10.1016/j.fusengdes.2010.12.084>.
- [7] D. Qu, W. Basuki, J. Gibmeier, R. Vaßen, J. Aktaa, Development of functionally graded tungsten/eurofer coating system for first wall application, *Fusion Sci. Technol.* 68 (2015) 578–581, <https://doi.org/10.13182/FST15-113>.
- [8] R. Vaßen, K.-H. Rauwald, O. Guillon, J. Aktaa, T. Weber, H. Back, D. Qu, J. Gibmeier, Vacuum plasma spraying of functionally graded tungsten/EUROFER97 coatings for fusion applications, *Fusion Eng. Des.* 133 (2018) 148–156, <https://doi.org/10.1016/j.fusengdes.2018.06.006>.
- [9] T. Emmerich, R. Vaßen, J. Aktaa, Thermal fatigue behavior of functionally graded W/EUROFER-layer systems using a new test apparatus, *Fusion Eng. Des.* 154 (2020), 111550, <https://doi.org/10.1016/j.fusengdes.2020.111550>.
- [10] T. Emmerich, D. Qu, B.-E. Ghidersa, M. Lux, J. Rey, R. Vaßen, J. Aktaa, Development progress of coating first wall components with functionally graded W/EUROFER layers on laboratory scale, *Nucl. Fusion* 60 (2020), 126004, <https://doi.org/10.1088/1741-4326/aba336>.
- [11] B.-E. Ghidersa, A.A. Sena, M. Rieth, T. Emmerich, M. Lux, J. Aktaa, Experimental investigation of EU-DEMO breeding blanket first wall mock-ups in support of the manufacturing and material development programmes, *Energies* 14 (2021) 7580, <https://doi.org/10.3390/en14227580>.
- [12] J. Klecka, J. Cizek, J. Matejíček, F. Lukac, J. Vala, Thick functionally-graded W-316L composite coatings for nuclear fusion applications, *Nucl. Mater. Energy.* 34 (2023), 101373, <https://doi.org/10.1016/j.nme.2023.101373>.
- [13] R. Neu, H. Maier, B. Bösow, S. Elgeti, H. Greuner, K. Hunger, J. Kondas, A. von Müller, Investigations on cold spray tungsten/tantalum coatings for plasma facing applications, *Nucl. Mater. Energy.* 34 (2023), 101343, <https://doi.org/10.1016/j.nme.2022.101343>.
- [14] G. Mauer, K.-H. Rauwald, Y.J. Sohn, Tungsten-steel functionally graded coatings for nuclear fusion applications manufactured by cold gas spraying, *J. Therm. Spray Technol.* 32 (2023) 375–387, <https://doi.org/10.1007/s11666-022-01503-z>.
- [15] T. Gräning, L. Tan, I. Robin, Y. Katoh, Y. Yang, A novel design of transitional layer structure between reduced activation ferritic martensitic steels and tungsten for plasma facing materials, *J. Mater. Res. Technol.* 24 (2023) 4285–4299, <https://doi.org/10.1016/j.jmrt.2023.04.019>.
- [16] T. Grammes, T. Emmerich, J. Aktaa, W/EUROFER functionally graded coatings for plasma facing components: technology transfer to industry and upscaling, *Fusion Eng. Des.* 173 (2021), 112940, <https://doi.org/10.1016/j.fusengdes.2021.112940>.
- [17] H. Neuberger, J. Rey, A. von der Weth, Francisco Hernandez, T. Martin, M. Zmitko, A. Felde, R. Niewöhner, F. Krüger, Overview on ITER and DEMO blanket fabrication activities of the KIT INR and related frameworks, *Fusion Eng. Des.* 96–97 (2015) 315–318, <https://doi.org/10.1016/j.fusengdes.2015.06.174>.
- [18] L.V. Boccaccini, L. Giancarli, G. Janeschitz, S. Hermsmeyer, Y. Poitevin, A. Cardella, E. Diegele, Materials and design of the European DEMO blankets, *J. Nucl. Mater.* (2004) 329–333, <https://doi.org/10.1016/j.jnucmat.2004.04.125>, 148–155.
- [19] P. Ennis, A. Czyska-Filemonowicz, Recent advances in creep-resistant steels for power plant applications, *Sadhana* 28 (2003) 709–730.
- [20] R. Lindau, M. Schirra, First results on the characterisation of the reduced-activation-ferritic-martensitic steel EUROFER, *Fusion Eng. Des.* 58–59 (2001) 781–785.
- [21] P. Ennis, A. Zielinska-Lipiec, O. Wachter, A. Czyska-Filemonowicz, Microstructural stability and creep rupture strength of the martensitic steel P92 for advanced power plant, *Acta Mater.* 12 (1997) 4901–4907.
- [22] K. Mergia, N. Boukos, Structural, thermal, electrical and magnetic properties of Eurofer 97 steel, *J. Nucl. Mater.* 373 (2008) 1–8, <https://doi.org/10.1016/j.jnucmat.2007.03.267>.
- [23] E. Gaganidze, *Material Property Handbook EUROFER97, EUROfusion Internal Document IDM2NZHBS, March 2020, EUROfusion, 2020.*
- [24] Warmfester Stahl X10CrWMoVNB9-2 Werkstoff-Nr. 1.4901, VdTÜV-Werkstoffblatt Nr. 552/3 (09.2009), 2009 (in German).
- [25] F. Tavassoli, Fusion Demo Interim Structural Design Criteria (DISDC) - Appendix A Material Design Limit Data - A3.S18E Eurofer Steel, CEA DEN-SAC DMN Technical Report DMN/DIR/NT/2004-02/A, 2004.
- [26] I. Zammuto, L. Giannone, A. Herrmann, A. Houben, A. Kallenbach, K. H. Schubbeck, B. Sieglin, S. Vorbrugg, Implementation of ferritic steel as in vessel wall: lessons learnt and follow up, *Fusion Eng. Des.* 124 (2017) 297–301, <https://doi.org/10.1016/j.fusengdes.2017.04.016>.
- [27] T. Emmerich, D. Qu, R. Vaßen, J. Aktaa, Development of W-coating with functionally graded W/EUROFER-layers for protection of First-Wall materials, *Fusion Eng. Des.* 128 (2018) 58–67, <https://doi.org/10.1016/j.fusengdes.2018.01.047>.
- [28] J. Matejíček, M. Vilémová, B. Nevrál, L. Kocmanová, J. Veverka, M. Halasová, H. Hadraba, The influence of substrate temperature and spraying distance on the properties of plasma sprayed tungsten and steel coatings deposited in a shrouding chamber, *Surf. Coat. Technol.* 318 (2017) 217–223, <https://doi.org/10.1016/j.surfcoat.2016.10.055>.
- [29] D. Qu, W. Basuki, J. Aktaa, Numerical assessment of functionally graded tungsten/EUROFER coating system for first wall applications, *Fusion Eng. Des.* 98–99 (2015) 1389–1393, <https://doi.org/10.1016/j.fusengdes.2015.06.120>.
- [30] A. Fischer-Cripps, *Introduction to Contact Mechanics. Chapter 11 - Depth-Sensing Indentation Testing.* Page 189-200, Springer, 2007.
- [31] DIN EN ISO 14577-1:2015 (German edition of ISO 14577-1:2015) Metallische Werkstoffe - Instrumentierte Eindringprüfung zur Bestimmung der Härte und anderer Werkstoffparameter - Teil 1: Prüfverfahren, 2015.

- [32] I. Choi, O. K. R. Schwaiger, Validity of the reduced modulus concept to describe indentation loading response for elastoplastic materials with sharp indenters, *J. Mater. Res.* 24 (2009) 998–1006, <https://doi.org/10.1557/jmr.2009.0120>.
- [33] T. Nozawa, H. Tanigawa, T. Kojima, T. Itoh, N. Hiyoshi, M. Ohata, T. Kato, M. Ando, M. Nakajima, T. Hirose, J.D. Reed, X. Chen, J.W. Geringer, Y. Katoh, The status of the Japanese material properties handbook and the challenge to facilitate structural design criteria for DEMO in-vessel components, *Nucl. Fusion* 61 (2021), 116054, <https://doi.org/10.1088/1741-4326/ac269f>.
- [34] Plansee Webpage on Tungsten, 2021. <https://www.plansee.com/en/materials/tungsten.html>. (Accessed 5 March 2021).
- [35] M. Rieth, M. Schirra, A. Falkenstein, P. Graf, S. Heger, H. Kempe, R. Lindau, H. Zimmermann, EUROFER97 - Tensile, Charpy, Creep and Structural Tests, FZKA 6911, Forschungszentrum Karlsruhe, 2003.
- [36] P. Fernández, A. Lancha, J. Lapeña, M. Serrano, M. Hernández-Mayoral, Metallurgical properties of reduced activation martensitic steel Eurofer97 in the as-received condition and after thermal ageing, *J. Nucl. Mater.* 307–311 (2002) 495–499.
- [37] B.L. Peng Duan, Zongde Liu, Jiayao Li, Xiangqian Tao, Study on microstructure and mechanical properties of P92 steel after high-temperature long-term aging at 650°C, *High Temp. Mater. Process.* 39 (2020) 545–555.
- [38] J. Davis (Ed.), Handbook of Thermal Spray Technology, Chapter 1 - Introduction to Thermal Spray Technology and Surface Science, ASM International, 2004, pp. 1–40.
- [39] D. Qu, Development of Functionally Graded Tungsten/EUROFER Coating Systems (PhD Thesis), PhD Thesis, Karlsruhe Institute of Technology, 2016, <https://doi.org/10.5445/IR/1000061922>.
- [40] A.-A.F. Tavassoli, A. Alamo, L. Bedel, L. Forest, J.-M. Gentzmittel, J.-W. Rensman, E. Diegele, R. Lindau, M. Schirra, R. Schmitt, H.C. Schneider, C. Petersen, A.-M. Lancha, P. Fernandez, G. Filacchioni, M.F. Maday, K. Mergia, N. Boukos, Baluc, P. Spätig, E. Alves, E. Lucon, Materials design data for reduced activation martensitic steel type EUROFER, *J. Nucl. Mater.* (2004) 329–333, <https://doi.org/10.1016/j.jnucmat.2004.04.020>, 257–262.
- [41] F. Tavassoli, Eurofer steel, development to full code qualification, *Procedia Eng.* 55 (2013) 300–308, <https://doi.org/10.1016/j.proeng.2013.03.258>.
- [42] A.-A.F. Tavassoli, J.-W. Rensman, M. Schirra, K. Shiba, Materials design data for reduced activation martensitic steel type F82H, *Fusion Eng. Des.* 61–62 (2002) 617–628, [https://doi.org/10.1016/S0920-3796\(02\)00255-7](https://doi.org/10.1016/S0920-3796(02)00255-7).
- [43] T. Hirose, T. Nozawa, R.E. Stoller, D. Hamaguchi, H. Sakasegawa, H. Tanigawa, H. Tanigawa, M. Enoda, Y. Katoh, L.L. Snead, Physical properties of F82H for fusion blanket design, *Fusion Eng. Des.* 89 (2014) 1595–1599, <https://doi.org/10.1016/j.fusengdes.2013.12.005>.
- [44] E. Gaganidze, Material Property Handbook Tungsten, EUROfusion Internal Document IDM2P3SPL, March 2020, EUROfusion, 2020.
- [45] F. Campbell (Ed.), Refractory Metals, ASM International, 2008, pp. 583–596.
- [46] A.S. Rabensteine, Mechanical Properties of Commercially Pure Sintered Tungsten Alloy Sheet from Room Temperature to 4500°F, The Marquardt Corporation, 1962.
- [47] H.-J. Kim, Y.-G. Kweon, Elastic modulus of plasma-sprayed coatings determined by indentation and bend tests, *Thin Solid Films* 342 (1999) 201–206.
- [48] S.-H. Leigh, C.-K. Lin, C. Berndt, Elastic response of thermal spray deposits under indentation tests, *J. Am. Ceram. Soc.* 80 (1997) 2093–2099.
- [49] W.B. Choi, L. Li, V. Luzin, R. Neiser, T. Gnäupel-Herold, H.J. Prask, S. Sampath, A. Gouldstone, Integrated characterization of cold sprayed aluminum coatings, *Acta Mater.* 55 (2007) 857–866, <https://doi.org/10.1016/j.actamat.2006.09.006>.
- [50] J. Nohava, R. Mušálek, J. Matějček, M. Vilémová, A contribution to understanding the results of instrumented indentation on thermal spray coatings — case study on Al₂O₃ and stainless steel, *Surf. Coat. Technol.* 240 (2014) 243–249, <https://doi.org/10.1016/j.surfcoat.2013.12.033>.
- [51] O. Kovarik, J. Cizek, J. Klecka, M. Karlik, J. Capek, J. Siegl, T. Chraska, S. Takayasu, Mechanical properties and fatigue crack growth in tungsten deposited by RF-plasma, *Surf. Coat. Technol.* 410 (2021), 126930, <https://doi.org/10.1016/j.surfcoat.2021.126930>.
- [52] L. Pawlowski, The Science and Engineering of Thermal Spray Coatings. Chapter 8 - Properties of Coatings, 2nd Ed, Wiley, 2008, <https://doi.org/10.1002/9780470754085.ch8>.
- [53] S. Heuer, J. Matějček, M. Vilémová, M. Koller, K. Illkova, J. Veverka, Th Weber, G. Pintsuk, J.W. Coenen, Ch Linsmeier, Atmospheric plasma spraying of functionally graded steel/tungsten layers for the first wall of future fusion reactors, *Surf. Coat. Technol.* 366 (2019) 170–178, <https://doi.org/10.1016/j.surfcoat.2019.03.017>.